砷化鎵及磷化銦異質接面雙載子電晶體

之銅金屬化製程研究

研究生：張尚文　　　　　　　　　　　　　　　　　　指導教授：張 翼 博士

國立交通大學材料科學與工程研究所

摘要

這篇論文為研究砷化鎵(GaAs)及磷化銦(InP)異質接面雙載子電晶體(HBT)之銅金屬化製程，內容包含了使用氮化鎢(WN_X)為擴散阻障層應用在磷化銦鎵/砷化鎵(InGaP/GaAs) HBT上，和不使用金材料而完全銅金屬化的InGaP/GaAs HBT，以及使用非合金材料的歐姆接觸和以鉑作為擴散阻障層應用在InP HBT上。

在銅的內連接導線方面，本篇使用濺鍍的方式分別成長氮化鎢和銅金屬材料做為擴散阻障層和內連接導線應用在InGaP/GaAs HBT上，從掃描式電子顯微鏡(SEM)、X光繞射(XRD)、歐傑電子光譜(AES)和片電阻(sheet resistance)的結果，銅/氮化鎢/氮化矽($Cu/WN_X/SiN$)和銅/氮化鎢/金($Cu/WN_X/Au$)的結構分別在550℃和400℃加熱後都還很穩定，並將元件施以55小時，高電流密度140 kA/cm^2之電流加速測試(current-accelerated test)，其電流增益並沒有下降，仍然超過100。另外，也將元件施以250 °C 25小時的熱處理，元件特性也並沒有明顯的改變。

之後我們更進一步利用鉑做為擴散阻障層成功製作出不使用金材料而完全銅金屬化的InGaP/GaAs HBT，使用鈀/鍺(Pd/Ge)和鉑/鈦/鉑/銅(Pt/Ti/Pt/Cu)做為n型和p型的歐姆接觸，使用鈦/鉑/銅(Ti/Pt/Cu)做為內連接導線金屬，從X光繞射和片電阻結果顯示Ti/Pt/Cu結構在350℃加熱後都還很穩定，將元件施以24小時，高電流密度140 kA/cm^2之電流加速測試，其電流增益並沒有下降，另外，也將元

件施以 250 °C 24 小時的熱處理，元件特性只有些微的改變。

最後我們更將銅製程應用在InP元件上，使用非合金材料鈦/鉑/銅(Ti/Pt/Cu)和鉑/鈦/鉑/銅(Pt/Ti/Pt/Cu)做為n型和p型的歐姆接觸，以及使用Pt做為擴散阻障層，成功製作出不使用金而完全使用銅金屬化的InP HBT。從歐傑電子光譜結果顯示Ti/Pt/Cu結構在 350℃加熱後都還穩定，將元件施以 24 小時，高電流密度 80 kA/cm^{2}之電流加速測試，其電流增益並沒有下降，也將元件施以 200 °C 3 小時的熱處理，元件特性幾乎改變。由以上的結果顯示，我們可以成功的製作出銅製程和完成電性研究，必且是第一次發表砷化鎵及磷化銦異質接面雙載子電晶體之銅金屬化製程。

The Study of Copper-Metallized GaAs and InP Heterojunction Bipolar Transistors

Student: Shang-Wen Chang Advisor: Dr. Edward Yi Chang

Department of Materials Science and Engineering

National Chiao Tung University

Abstract

In this dissertation, copper-metallized GaAs and InP heterojunction bipolar transistors (HBTs) were studied. The developed copper metallization technology for HBTs include interconnect copper metallization of InGaP/GaAs HBTs using WN_X as the diffusion barrier, gold-free fully Cu-metallized InGaP/GaAs HBTs, and gold-free fully Cu-metallized InP HBTs using non-alloyed ohmic and platinum diffusion barrier.

The WN_X and Cu films were deposited sequentially on the InGaP/GaAs HBT wafers as the diffusion barrier and interconnect metallization layer respectively using the sputtering method. As judged from the data of scanning electron microscopy (SEM), X-ray diffraction (XRD), Auger electron spectroscopy (AES), and sheet resistance, the Cu/WN_X/SiN and Cu/WN_X/Au structures were very stable up to 550℃ and 400℃ annealing, respectively. Current accelerated stress test was conducted on the Cu/ WN_X metallized HBTs with V_{CE}=2 V, J_C=140 kA/cm^2 and stressed for 55 hours, the current gain (β) of these HBTs showed no degradation and was still higher than 100 after the stress test. The Cu/ WN_X metallized HBTs were also thermally annealed at 250℃ for 25 hours and showed no degradation in the device characteristics after the annealing.

Gold-free, fully Cu-metallized InGaP/GaAs HBTs using platinum as the diffusion barrier have also been successfully fabricated. The gold free HBTs use Pd/Ge and Pt/Ti/Pt/Cu as n^+-type and p^+-type ohmic contact metals, respectively, and use Ti/Pt/Cu as interconnect metals with platinum as the diffusion barrier. The Ti/Pt/Cu structure was stable after annealing up to 350℃ as judged from the XRD and the sheet resistance data. A current-accelerated stress test was conducted on the device with a current density J_C=140 kA/cm^2 for 24 h, the current gain of the device showed no degradation after the stress. The devices were also thermally annealed at 250℃ for 24 h and showed little change.

In addition, gold-free, fully Cu-metallized InP HBTs using non-alloyed Ti/Pt/Cu and Pt/Ti/Pt/Cu ohmic contacts and platinum diffusion barrier have been successfully fabricated. The InGaAs/Ti/Pt/Cu ohmic structure used in this study was very stable after annealing up to 350 ℃ as judged from the Auger depth profiles. A current-accelerated stress test was conducted on the device with a current density J_C=80 kA/cm^2 for 24 hours, and the current gain showed no degradation after the current stress. The devices were also thermally annealed at 200℃ for 3 hours and showed almost no change in the electrical parameters after the heat treatment. Overall, we have successful developed the copper metallization process for the GaAs and InP HBTs and have reported for the first time the fabrication and electrical performance of the Cu-metallized GaAs and InP HBTs.

誌謝

要感謝許多人的幫忙，才能使本論文能夠如期的完成。首先要感謝我的指導教授張翼博士，在我博士班的研究生活當中，帶領我進入砷化鎵高頻元件的領域，提供完整的訓練及儀器資源，使我能夠成功的建立實驗室第一批異質接面雙載子電晶體的製程，非常難得可貴的經驗，受用無窮。

其次我要感謝李承士博士、陳仕鴻博士、張晃崇博士、羅廣禮博士、方照詒博士在實驗製程以及材料分析上提供寶貴的經驗以及建議，使我降低許多摸索的時間，也要感謝楊宗熺博士及林岳欽博士在實驗上的建議和電性上面的幫忙，一起陪伴我走過五年的博士研究。還有要感謝國家奈米實驗室(NDL)及交大半導體中心，提供優良的儀器設備與環境，使實驗能夠順利進行。

另外我也要感謝陳克弦同學、連亦中同學、褚立新同學、李晃銘同學、吳偉誠同學、林立偉同學、曾昭瑋同學、謝東霖同學在實驗上的幫忙協助，以及詹前璋先生、梁坊旭先生在儀器設備及廠務方面的幫忙，還有感謝李澤倫先生、張俊偉學長、謝炎璋同學、黃瑞乾同學、徐金鈺同學、吳雲驥同學、彭怡瑄同學、呂宗育同學、葉協鑫同學、邵宜瑄同學、曾建堯同學以及其他歷年來許多實驗室的同學在背後默默的幫助我，還有感謝蘇筠雯小姐及莊蕙菁小姐在行政方面的協助幫忙。

最後，我要特別感謝我的父母親、家人以及陪伴我七年多的女友玉清，感謝您們的關心、支持、包容與鼓勵，使我無後顧之憂，能夠專心順利完成學業，願這份榮耀與您們分享。

Contents

Abstract (in Chinese)……………………………………………….…i

Abstract (in English)……………………………………………iii

Acknowledge (in Chinese)……………………………………………v

Contents……………………………………………………………vi

Table Captions…………………………………………………….…ix

Figure Captions………………………………………………….…x

Chapter 1 Introduction……………………………………………1

1.1 General Background and Motivation………….…………………………..1

1.2 Outline of the Dissertation………………………………………………....3

Chapter 2 Fabrication of Heterojunction Bipolar Transistor……..…6

2.1 Introduction of GaAs HBT………….…………………………………..6

2.2 Introduction of InP HBT………..………………………………………8

2.3 Device Structure..……………………...……………………………………10

2.4 Device Fabrication…………………………………………………..10

2.4.1 Emitter Mesa, Collector Mesa, and Isolation……………………………..11

2.4.2 Emitter and Collector Ohmic Contact Metal……………………………...11

2.4.3 Base Ohmic Contact Metal………………………………………………12

2.4.4 Device Passivation and Contact Via………………………………………12

2.4.5 Interconnect Metal Line…………………………………………………..13

Chapter 3 Use of WN_X as the Diffusion Barrier for Interconnect Copper Metallization of InGaP/GaAs HBTs……………………….....25

3.1 Introduction…………………………………………………………..25

3.2 Experimental…………………………………………………………...26

3.3 Material Stability of the Diffusion Barrier……………………..……………...28

3.4 Device Electrical Characteristics……………………………………………30

3.5 Conclusion………………...…………………………………………………32

Chapter 4 Gold-Free Fully Cu-Metallized InGaP/GaAs Heterojunction Bipolar Transistor……………………………………....47

4.1 Introduction…………………………………………………………………..47

4.2 Experimental………………………………………………………...……48

4.3 Ohmic Contact Result………………………………………………………50

4.4 Thermal Stability of Ti/Pt/Cu Multilayers…………………..………………50

4.5 Device Electrical Characteristics……………………………………………51

4.6 Conclusion…………………………………...……………………………53

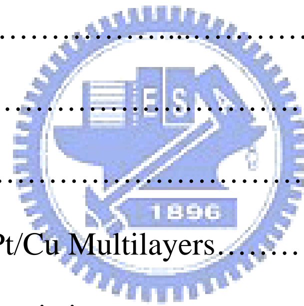

Chapter 5 A Gold-Free Fully Cu-Metallized InP HBT Using Non-Alloyed Ohmic Contact and Platinum Diffusion Barrier…........66

5.1 Introduction……………………..……………………………..…………66

5.2 Experimental…………………………………………………………………67

5.3 Ohmic Contact Result……………………….………………………………69

5.4 Thermal Stability of the Pt Diffusion Barrier……………….………………70

5.5 Device Electrical Characteristic……………………………….………….....71

5.6 Conclusion……………………………..……………………………………..73

Chapter 6 Conclusions……………………..………………………87

Reference………………………………………………………………89

Vita (in Chinese)

Publication List

Table Captions

Chapter 1

Table 1.1 Properties comparisons of the possible interlayer metals.

Chapter 2

Table 2.1 Band-gap information of different heterostructures.

Table 2.2 The typical epitaxial layer structure of the InGaP/GaAs HBT.

Table 2.3 The typical epitaxial layer structure of the InP/InGaAs HBT.

Chapter 5

Table 5.1 Comparisons of the ohmic contacts on n-type and p-type InGaAs materials.

Figure Captions

Chapter 2

Figure 2.1 Schematic of the cross section of an HBT structure.

Figure 2.2 Energy band diagram of an HBT structure.

Figure 2.3 The band diagrams of (a) a homojunction bipolar transistor and (b) a heterojunction bipolar transistor.

Figure 2.4 Energy-band band lineups for the two abrupt interfaces:(a) InP/$In_{.53}Ga_{.47}As$ and (b) $Al_{.48}In_{.52}As$/ $In_{.53}Ga_{.47}As$.

Figure 2.5.1 Emitter mesa etch.

Figure 2.5.2 Base and collector mesa etch.

Figure 2.5.3 Mesa isolation.

Figure 2.5.4 Emitter and collector ohmic contact metal formation.

Figure 2.5.5 Base ohmic contact metal formation.

Figure 2.5.6 Silicon Nitride Deposition.

Figure 2.5.7 Nitride via etch.

Figure 2.5.8 Interconnect metal line.

Figure 2.6 SEM image of HBT.

Chapter 3

Figure 3.1 Cross section of the InGaP/GaAs HBT with interconnect Cu metallization.

Figure 3.2 AES depth profiles of the Cu/WN_X/Au samples (a) as deposited; (b) after 400℃ annealing; and (c) after 450℃ annealing.

Figure 3.3 SEM images of the Cu/WN_X/Au samples (a) as deposited and (b) after 450 ℃ annealing.

Figure 3.4 XRD patterns of the $Cu/WN_X/Au$ samples as deposited and after annealing at various temperatures.

Figure 3.5 Sheet resistance of the $Cu/WN_X/SiN/GaAs$ samples as deposited and after annealing at various temperatures.

Figure 3.6 AES depth profiles of the $Cu/WN_X/SiN/GaAs$ samples (a) as deposited; (b) after 550℃ annealing; and (c) after 600℃ annealing.

Figure 3.7 XRD patterns of the $Cu/WN_X/SiN$ samples as deposited and after annealing at various temperatures.

Figure 3.8 Comparison of the typical I_C-V_{CE} characteristics for the emitter area (3×20 μm^2) HBTs with Cu and with Au interconnect metallizations.

Figure 3.9 Comparison of the Gummel plots for the emitter area (3×20 μm^2) HBT with Cu and with Au interconnect metallization.

Figure 3.10 Current gain as a function of the stress time at a constant I_B for the emitter area (3×20 μm^2) HBTs with Cu and Au interconnect metallization.

Figure 3.11 Gummel plots measured before and after 55 hours current accelerated stress test with high current density of 140 kA/cm^2 for the emitter area 3×20 μm^2 HBT devices (a) with Cu interconnect metallization and (b) with Au interconnect metallization.

Figure 3.12 Common emitter I-V curves measured before and after 250℃ 25 hours annealing for the emitter area 3×20 μm^2 HBT devices (a) with Cu interconnect metallization and (b) with Au interconnect metallization.

Figure 3.13 Gummel plots measured before and after 250℃ 25 hours annealing for the emitter area 3×20 μm^2 HBT devices (a) with Cu interconnect metallization and (b) with Au interconnect metallization.

Chapter 4

Figure 4.1 Cross section of the Au-free fully Cu-metallized InGaP/GaAs HBT.

Figure 4.2 Specific ohmic contact resistance for the n^+-GaAs/Pd/Ge structure.

Figure 4.3 Specific ohmic contact resistance for the p^+-GaAs/Pt/Ti/Pt/Cu structure.

Figure 4.4 Sheet resistance of the GaAs/Ti/Pt/Cu samples as-deposited and after annealing at various temperatures.

Figure 4.5 XRD patterns of the Ti/Pt/Cu samples as-deposited and after annealing at various temperatures.

Figure 4.6 Comparison of the typical I_C-V_{CE} characteristics of the fully Cu-metallized and the conventional Au-metallized 4×20-μm-emitter-area HBTs.

Fig. 4.7 Comparison of the Gummel plots for the emitter area (3×20 μm^2) HBT with Cu and with Au interconnect metallizations.

Figure 4.8 Current gain as a function of stress time at constant I_B for the 4×20-μm-emitter-area fully Cu-metallized HBT.

Figure 4.9 Common emitter I-V curves measured before and after annealing at 250℃ for 24 h for the 4×20-μm-emitter-area fully Cu-metallized HBT without silicon nitride protective layer.

Figure 4.10 Common emitter I-V curves measured before and after annealing at 250℃ for 24 h for the 4×20-μm-emitter-area fully Cu-metallized HBT with silicon nitride protective layer.

Figure 4.11 Current gain H_{21} curves measured before and after annealing at 250℃ for 24 h for the 4×20-μm-emitter-area fully Cu-metallized HBT.

Chapter 5

Figure 5.1 Cross section of Au-free fully Cu-metallized InP/InGaAs HBT.

Figure 5.2 Multilayer structures of (a)n+InGaAs/Ti/Pt/Cu and (b)n+InGaAs/SiN/Ti/Pt/Cu.

Figure 5.3 Specific ohmic contact resistances (a) on n+-InGaAs (b) on p+-InGaAs after annealing at various temperatures.

Figure 5.4 AES depth profiles of the Cu/Pt/Ti/InGaAs sample (a) as deposited; (b) after 350℃ 30 min annealing; (c) after 400℃ 30 min annealing.

Figure 5.5 SEM micrographs of the samples (a) as-deposit, and annealing at temperatures of (b) 300℃, (c) 350℃, and (d) 400℃.

Figure 5.6 Sheet resistance results of the InGaAs/SiN/Ti/Pt/Cu multilayer samples as-deposit and after annealing at various temperatures.

Figure 5.7 The typical common emitter current I-V characteristics of the 3× 20-μm-emitter-area Au free fully Cu-metallized InP HBT.

Figure 5.8 Current gain as a function of stress time at constant I_B for 3× 20-μm-emitter-area fully Cu-metallized InP HBT.

Figure 5.9 Common emitter I-V curves measured before and after annealing at 200℃ for 3 h for the 3×20-μm-emitter-area fully Cu-metallized InP HBT.

Figure 5.10 Cutoff frequency (f_T) as a function of base current (I_C) for the 3×20 μm^2 emitter area InP HBTs with fully Cu metallization (a) before annealing and (b) after 3 hours annealing.